วารสารวิศวกรรมศาสตร์และนวัตกรรม
Journal of Engineering and Innovation

บทความวิจัย

A comparative study on removal of malachite green dye using activated carbons from bituminous coal and coconut shells

Chakkrit Umpuch* Kamonlak Lerdsri Gullanat Hansamer Pongpapas Phosai Wanphaka Chaowiang Wanwisa Sittawaong Channarong Puchongkawarin

Department of Chemical Engineering, Faculty of Engineering, Ubon Ratchathani University Ubon Ratchathani 34190

* Corresponding author.

E-mail: chakkrit.u@ubu.ac.th; Telephone: 0 4535 3343

Received 9 May 2022; Revised #1 1 September 2022; Accepted 22 September 2022

Abstract

Adsorption of malachite green (MG) dyes on the mesoporous activated carbon made from the bituminous coal (AC1) and the microporous activated carbon made from coconut shells (AC2) was comparatively studied. Two adsorbents were characterized to study the specific surface area and porosity, surface functionalities, textural morphology, and elemental analysis. Subsequently, the influence of affecting factors on adsorption was evaluated. The highest adsorption capacity was found at initial pH of 4.0–8.0, contact time of 30 min, initial dye concentration of 300 mg/L, and temperature of 30-50 °C. The adsorption of MG dyes on both adsorbents were explained by the Langmuir isotherm with the maximum adsorption capacities of 131.58 mg/g for the AC1 and 54.65 mg/g for the AC2. The adsorption kinetics followed the pseudo-second order reaction model. Although the AC1 has higher MG dye uptake than that of AC2, both are effective adsorbents for MG removal from dye effluents.

Keywords

malachite green; activated carbon; bituminous coal; coconut shell; adsorption

1. Introduction

Nowadays, large quantities of synthetic dyestuffs are used in many industries such as textile, leather, cosmetics, paper, printing, plastic, pharmaceuticals, food, etc [1]. Although these dyes are used to produce bright and long-lasting colour products, they can potentially contaminate water resources and generate wastewater. Wastewater or effluent containing these dyes causes unsightly aesthetic issues, a reduction in sunlight transmission into the water bodies, and less photosynthetic action. The dye effluent may contain chemicals that exhibit inhibition towards microbial populations and can be toxic and/or carcinogenic to mammals [2]. The malachite green (MG) dye has been widely used for dyeing materials such as silk, wool, paper, and leather due to its low cost, easy availability, and efficacy [3]. The MG is, however, toxic to a wide range of aquatic and terrestrial animals. It causes damage to the liver, spleen, kidney, and heart; inflicts lesions on the skin, eyes, lungs, and bones; and produces teratogenic effects [4]. It is difficult to remove the MG from the aqueous solutions because it is highly resistant to biodegradation resulting from its complex structure

and long-term stability in the wastewater [5]. Therefore, a proper treatment of the effluent contaminated with the MG is becoming extremely important.

Over decades, various methods have been employed for dye removal from the liquid media, categorized into 3 approaches: physical, chemical, and biological approaches. The physical methods include coagulation and flocculation, ion exchange, irradiation, and membrane filtration [6]. The chemical processes consist of advanced oxidation, electrochemical destruction, Fenton reaction, ozonation, and photochemical ultraviolet irradiation [7]. Examples of the biological methods include algae degradation, enzyme degradation, fungal cultures, and microbial culture [8]. Among them, the adsorption process has received much attention because of its low cost, and ease of application [9]. Activated carbon is a well-known adsorbent that shows high efficacy for dye removal due to its high specific surface and porosity. Various carbonaceous materials such as hard shells of apricot stones, almond, walnut, and hazelnut shells, rice hulls, coconut shells, coal, and wood can be used as precursors for preparation of the activated carbon [10].

Preparation of the activated carbon can be divided into two stages: carbonization and activation. In the first stage, the carbonaceous material is burnt under an air-free condition deriving the carbon-rich residue and eliminating the bulk of the volatile matter. After that the char residue is activated to increase the number of pores through physical and chemical activations. The physical activation is carried out to release CO_2 by burning the char again at a temperature between 700 – 900 °C in presence of activating agents such as CO_2, steam, and air [11]. On the other hand, the chemical activation is done by impregnating the char with a concentrated solution of a dehydrating compound e.g. KOH, H_3PO_4, H_2SO_4, and $ZnCl_2$ and then reheating at a temperature between 400-750 °C under the air-free condition [12]. Although the chemical activation is done at a lower temperature in comparison with the physical activation, the removal of the remaining dehydrating compound on the activated carbon is additionally required.

The activated carbon derived from coconut shells exhibits plenty of micropores, the smallest type of pores, which can adsorb volatile organic compounds and other impurities from drinking water [13]. A high surface area with a large portion of micropores, high hardness with low dust generation, and a renewable and green material are some advantages of the activated carbon from coconut shells [14]. The activated carbon from the coconut shells can be used as an adsorbent for the removal of cationic dyes from liquid media including rhodamine B with the highest adsorption capacity of 19.5 mg/g [15] and methylene blue with the maximum adsorption capacity of 320.5 mg/g [16]. In addition, the activated carbon made from the bituminous coal has a wide range of pore diameters containing mainly mesoporous as well as micropores [17]. It is used for the removal of various organic chemical contaminants in water. The advantages of the activated carbon-based bituminous coal include being used as filter media for fluid, consistent density, a hard material with minimal dust generation, and being economical. The activated carbon from a bituminous coal can be used as an effective adsorbent for dyes from aqueous solution such as the basic blue 41 dye with highest adsorption capacity of 460 mg/g [18] and methylene blue with the maximum adsorption capacity of 580 mg/g [19].

A recent study comparing the removal of MG using four different activated carbons was published [20]. However, the comparison was limited to activated carbon with same pore size range, i.e., mesoporous activated carbon compared to other mesoporous activated carbons. To our knowledge, there has never been a study that compares the removal of MG by mesoporous and microporous activated carbons, which is claimed as a novelty in this study. The purpose of this study is to examine the physical properties of two commercially available activated carbons generated from bituminous coal and coconut shells. To evaluate the adsorption capabilities, batch adsorption tests were conducted as a function of contact time, initial pH solution, initial dye concentration, and temperature. After that, an efficiency comparison of two activated carbons for dye removal was carried out. The experimental results were fitted to well-established kinetics and adsorption isotherm models, respectively, to acquire a better understanding of the adsorption mechanisms and behavior.

2. Materials and Methods

2.1 Chemicals

MG ($C_{23}H_{25}N_2$), with a molecular weight of 364.911 g/mol, was provided by SIGMA-Aldrich. It is also known as basic green. The chemical structure of the MG is depicted in Figure 1, which was obtained from the supplier's product information sheet. All substances were used without any sort of purification. The activated carbon from the bituminous coal (Pure sorb WB90 brand) with an iodine number of 900 (ASTM D 4607-94 test method) was obtained from the Green Power Nature Co., Ltd, Thailand. The activated carbon from coconut shells (Eunicarb brand) with an iodine number of 900 (ASTM D 4607-94 test method) was purchased from the Filter Supply Co., Ltd, China.

2.2 Activated carbon preparation

The activated carbons were dried in an oven at 105 °C until they were uniform in weight. They were then crushed and sorted through a sieve with a mesh size of 100. AC1 stands for activated carbon made from bituminous coal, whereas AC2 stands for the activated carbon from coconut shells. A desiccator was used to preserve two activated carbons for further use. Various approaches were used to characterize both activated carbons at first. For example, the BET-method, BJH technique, and N2 adsorbed volume at a relative pressure of 0.99 were used to calculate specific surface area, pore size, and total pore volume were evaluated from the N2 adsorption-desorption isotherm at 77 K. Fourier-Transform Infrared Spectroscopy (FTIR) was used to determine the surface functionalities of the adsorbents. Scanning Electron Microscopy (SEM) images were used to examine the adsorbent's textural morphology, and elemental composition was assessed using Energy Dispersive X-ray Spectroscopy (EDS).

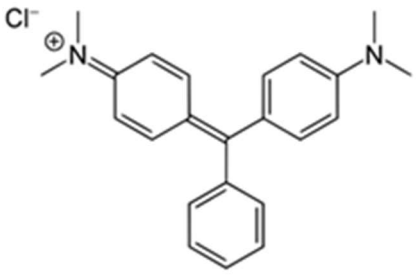

Figure 1 Chemical Structure of MG [3]

2.3 Batch tests

Batch adsorption studies were conducted as a function of the contact time, initial pH, initial dye concentration, and temperature. First, the effect of

the contact time was investigated. A set of Erlenmeyer flasks was made with 50 mL of 150 mg/L dye solutions. The initial pH of dye solutions was set to 3.0 from the start. The solutions were mixed with 0.1 g of adsorbents and then shaken at 30 °C. The samples were taken at 10– 180 minute intervals and measured. The adsorbents were removed from the suspension using vacuum microfiltration, and the filtrate was tested using a UV Vis Spectrophotometer with a maximum wavelength (λmax) of 512 nm to determine absorbance. Using the calibration curve, the absorbance was converted to the dye concentration (a plot of absorbance vs. dye concentration). Second, the influence of initial pH was studied. To obtain an initial concentration of 50 mg/L, several identical- size Erlenmeyer flasks were filled with 50 mL of the dye solution. By adding 0.1 M NaOH and/ or 0. 1 M HCl, the pH of the solutions was changed from 2.0 to 10.0. For each experiment, 0.1 g of the adsorbent was added to the dye solution, which was then agitated for 24 hours at a regulated temperature of 30 °C. The final dye concentration was determined in the same way as in the previous studies. Third, another set of Erlenmeyer flasks containing 50 mL of dye solutions ranging from 50 to 300 mg/L were created to investigate the influence of starting dye concentration. The dye solutions were started with a pH of 4.0. The concentration of the analysis process followed the same pattern as the previous studies. Finally, the influence of temperature on adsorption was investigated. The final experiment was conducted in the same way as the first and third, but the temperature was varied from 30 °C to 40 °C and 50 °C, respectively.

3. Results and Discussions

3.1 Characteristics of adsorbents

The N2 adsorption–desorption isotherms at 77 K of activated carbons from the bituminous coal (AC1) and coconut shells (AC2) are shown in Figure 2. The hysteresis loop was detected on the N2 adsorption-desorption isotherm of the AC1, which was classified as type IV by the IUPAC. The type IV isotherm is widely encountered in the characterization of the mesoporous materials [21]. The hysteresis loop, on the other hand, was not observed in the AC2's N2 adsorption- desorption isotherm, which was categorized as a type I isotherm by IUPAC. The N2 absorbed and N2 desorbed in the micropore at a relative pressure are normally identical as an overlapping line of AC2 in Figure 2. However, the N2 adsorbed in the mesopore becomes N2 liquid, which needs more vacuum to release the N2 liquid from the mesopore. This results in a deviation of the adsorption-desorption as illustrated by a hysteresis loop of AC1 in Figure 2. In the characterization of microporous materials, the type I isotherm is frequently encountered [22].

The BET technique determined that the AC1 had a specific surface are of 694.60 m2/g while the AC2 had a specific surface area of 579.3 m2/g. The AC1 has a higher specific surface than the AC2 by 16.5 percent. The AC1 and AC2 have the same average pore size of 1.80 nm, which were obtained from the Barret-Joyner-Halenda (BJH) method. The AC1 pore distribution, on the other hand, is wider than the AC2. A substantial fraction of micropores found on the adsorbent surface is activated carbon with an average pore size less than 2 nm. Furthermore, the total pore volumes of the AC1 and AC2 were 8.02x10-2 and

1.48x10-2 cm3/g, respectively, based on the volume of N2 adsorbed at a relative pressure of 0.99.

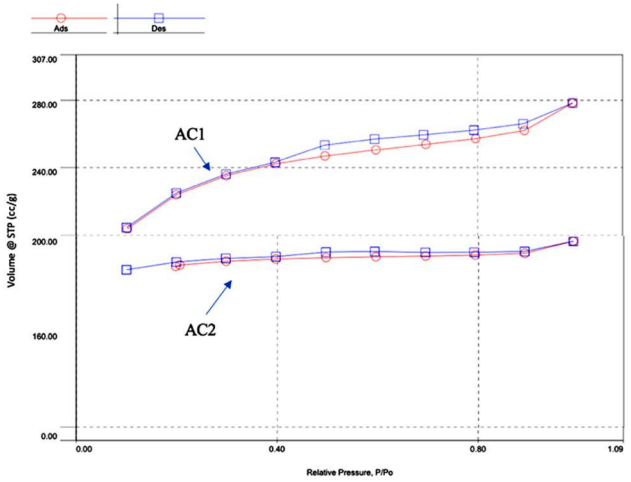

Figure 2 N_2 adsorption- desorption isotherm at 77 K of AC1 and AC2 (Ads (red line) stands for adsorption and Des (blue line) stands for desorption.)

The surface functions of the AC1 and AC2 were assessed using the IR spectra shown in Figure 3. The vibrations or stretching of bonds on the AC1 and AC2 caused the adsorption bands to be observed. The vibration bands at 3,433 cm-1 assigned to O-H stretching (alcohols Phenols), 2,920 cm-1 assigned to C-H stretching, 1,573 cm-1 assigned to C=O stretching, 1,043 cm-1 assigned to C-O stretching, 563 cm-1 assigned to C-Cl and 477 cm-1 assigned to C-Br stretching were observed in the IR spectra of the AC1 [23]. Hydrophobic interactions, as well as carboxyl and alcohol groups linked to AC1's exterior surface, were predicted. The vibration bands at 3,451 cm-1 were assigned to O-H stretching (alcohols Phenols), 1,572 cm-1 to C=O stretching (alkane), and 1,220 cm-1 to C-C stretching in the IR spectra of the AC2 [24]. The surface functionalities, presenting on the AC1's external surface, were likewise found on the AC2's surface. There are two types of interactions between the activated carbons and the MG. The weak interactions or van der Waals forces between carbons and other adsorbate molecules, are first. The second type is strong interactions, such as 1) hydrogen bonds with electrostatic forces between carboxyl groups and the positively charged molecules, 2) the hydrophobic interactions between AC1 and AC2 hydrophobic sectors and MG hydrophobic sectors, and 3) pi-pi stacking interactions between aromatic rings of activated carbon structure and the hydrophilic part of MG [25].

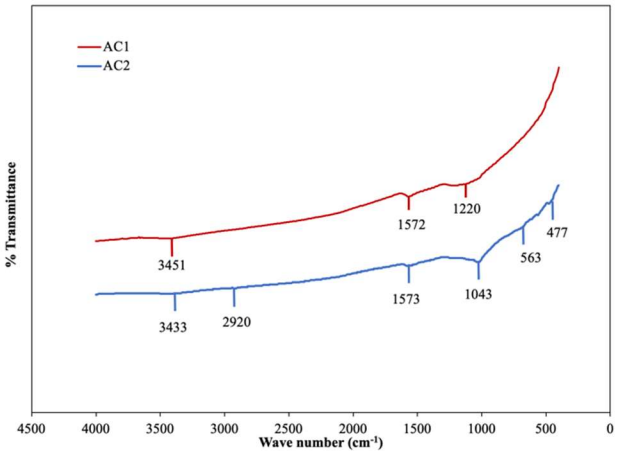

Figure 3 FTIR spectra of AC1 and AC2

SEM images of both adsorbents at various magnifications are shown in Figure 4. At a magnification of 500x, Figures 4A and 4D show the textural surfaces of the AC1 and AC2, displaying cracks, fissures, and pores of varied sizes spread across the surfaces. At 1,000x magnification, different sizes of pores were identified in both A1 (Figure 4B) and AC2 (Figure 4E). Figure 4C is a 10,000x magnification SEM image exhibiting the distribution of similar-sized pores along the smooth surface of the AC1. Crystals of various sizes deposited on the smooth surface and collected inside the massive pores are depicted in Figure 4F. Comparable carbonaceous compounds produced similar findings [26].

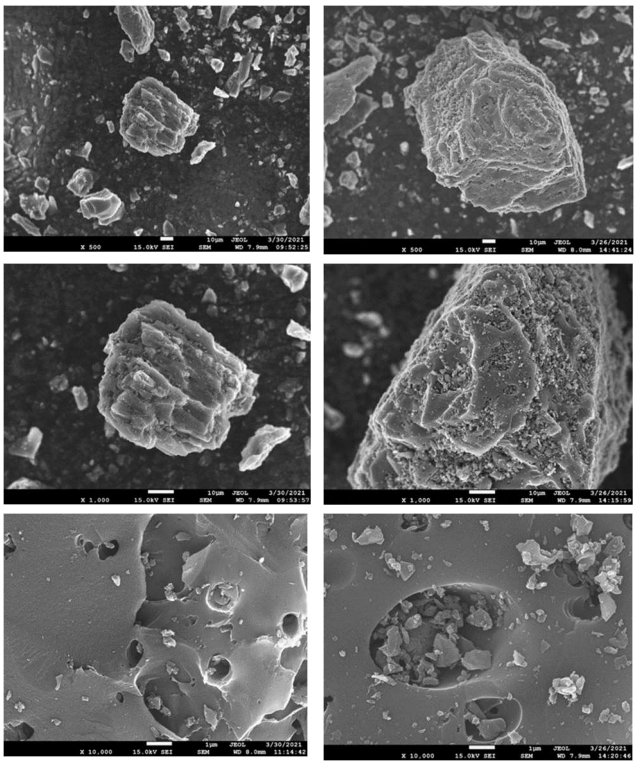

Figure 4 SEM images of AC1 at (A: top left) 500x, (B: middle left) 1000x, and (C: bottom left) 10,000x magnifications and AC2 at (D: top right) 500x, (E: middle right) 1000x, and (F: bottom right) 10,000x magnifications

The elemental compositions of AC1 and AC2 as determined by the EDS are shown in Figure 5. The carbon content of the AC1 (Figure 5A) was 76.10 percent by weight, 16.70 percent weight oxygen, 1.65 by weight sodium, 3.09 percent by weight aluminum, and 2.46 percent by weight silicon. According to the EDS analysis, the AC2 (Figure 5b) contains 94.45 percent by weight carbon, 4.39 percent by weight oxygen, and 1.16 percent by weight potassium. The AC2 looks to have a significantly larger carbon content than the AC1. Activated carbons have variable elemental compositions depending on how they are generated from various sources [27]. Because bituminous coal has more heterogeneous components than coconut shells, the AC1 has a lower carbon content.

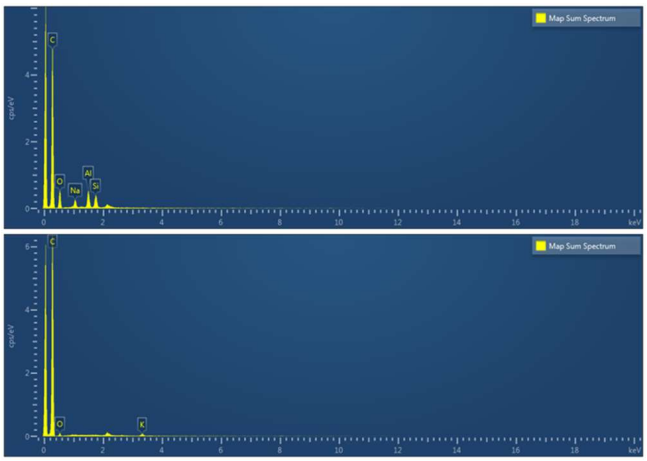

Figure 5 EDS pattern of AC1 (top) and AC2 (bottom)

3.2 Influence of Affecting factors on adsorption

3.2.1 Effect of contact time

Enhanced contact duration increased MG adsorption on both AC1 and AC2, as shown in Figure 6. After the first 5 minutes, the adsorption rate was quick, then slower for the next 5-30 minutes, and finally steady after 30 minutes. The rapid increase in the first stage is due to the large number of adsorptive sites available on the exterior surfaces of the adsorbents for extracting the MG from the solution [28]. The MG molecules can easily occupy these surfaces. Following that, in the second stage, the greater MG concentration difference between the saturated exterior surfaces and the adsorbent interior induces MG molecules to diffuse into the pores of both adsorbents. Due to the influence of the internal mass transfer resistance, the diffusion rate in the second stage was slower than in the first [29]. After 30 minutes, both adsorbents' dye uptakes leveled off in the final stage. At the equilibration stage of 30 minutes, both adsorbent's dye uptakes leveled off in the final stage. At the equilibration stage of 30 minutes, all adsorptive sites of the adsorbents, including exterior and internal surfaces, were occupied by MG molecules.

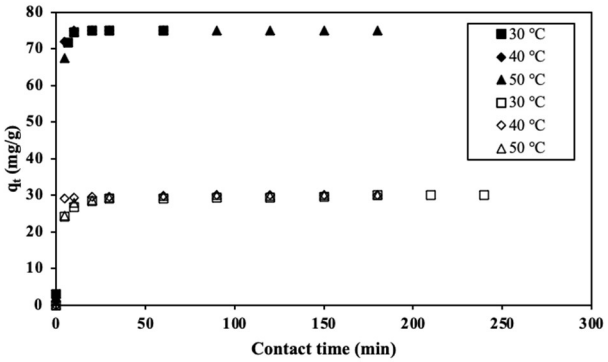

Figure 6 Adsorption capacity of MG on AC1 (full symbol) and AC2 (empty symbol) vs. contact time

3.2.2 Effect of initial pH solution

With an increase in the initial pH, both AC1 and AC2 adsorption capabilities rose (Figure 7). Because of the presence of acidic functional groups, the surfaces of both AC1 and AC2 were shown to be negatively charged (carboxylic acid and alcohol). The negatively charged surface had a strong affinity to cationic MG molecules at low pH. Due to competing adsorption between the H^+ ions and the MG molecules on the adsorption sites, the presence of H^+ ions in the acidic pH solution induces poor MG uptake. The acidic functional groups were dissociated at higher pH, and the surfaces of both AC1 and AC2 were found to be negative, resulting in increased adsorption capabilities. For the AC1 and AC2, the pH of the point of zero charge (pH_{pzc}) was found to be 4.8 and 2.0, respectively [26, 30]. The carbon surface gains negative charges at pH > pH_{pzc}, which favors the adsorption of cationic species like MG molecules. The MG molecules connect with the negative surfaces of both AC1 and AC2 via electrostatic interactions. Furthermore, in an alkaline media, the concentration of H^+ falls, making adsorption between MG dyes and H^+ ions less competitive.

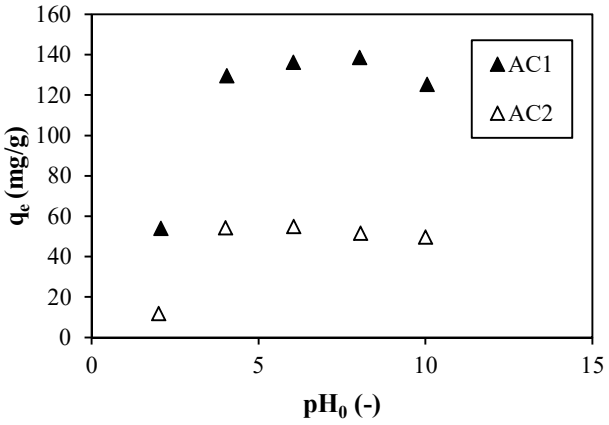

Figure 7 Adsorption capacity of MG on AC1 (full symbol) and AC2 (empty symbol) vs. initial pH solution

3.2.3 Effect of initial dye concentration

An increase in the initial MG dye concentration induced the increases in MG dyes adsorbed on both AC1 and AC2 (Figure 8). The larger concentration gradient (driving force) between the external surface and the interior of the adsorbents is responsible for this. Internal mass transfer resistance is reduced, allowing MG species to permeate deeper into the pores. As a result, a higher number of MG dyes were adsorbed at the higher starting dye concentration, which was consistent with previous research [31-32].

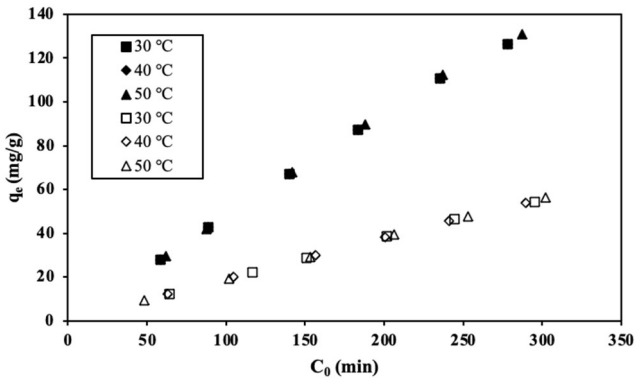

Figure 8 Adsorption capacity of MG on AC1 (full symbol) and AC2 (empty symbol) vs. initial dye concentration

3.2.4 Effect of temperature

As illustrated in Figure 6 and 8, the amount of dye molecules adsorbed on AC1 and AC2 was unaffected by temperature. This means that the adsorption is of a physical origin, with van der Waals, hydrogen bonding, and / or electrostatic attraction as the primary interactions. Furthermore, no chemical reaction is involved in this study' s adsorption procedure. The maximum MG adsorption capabilities were 138.56 and 54.95 mg/g on the AC1 and AC2, respectively, at pH0 of 4.0-8.0, contact period of 30-minute, dye concentration of 300 mg/L, and 30 – 50 °C, according to the above data. The AC1 adsorbed 60 percent more MG than the AC2. This may be due to the AC1 having a larger specific surface area and total pore capacity than the AC2.

3.3 Kinetic adsorption modelling

The pseudo- first order reaction and pseudo-second order reaction models are two kinetic models used to predict the rate of limiting step. Lagergren [33] suggested a pseudo-first order reaction model based on the assumption that the rate-limiting step is the sharing of electrons between the adsorbent and adsorbate on the adsorbent surface. The model expression's linearized form is given by:

$$ln(q_e - q_t) = ln(q_e) - k_1 t \quad (1)$$

The adsorption capacities at the equilibrium stage and at instantaneous time t, respectively, are q_e and q_t (mg/g). The pseudo-first order rate constant (1/min) is denoted by k_1. Adsorption involves chemical reactions if the experimental results fit the pseudo-first order reaction model, this model usually fits the first 30 minutes of experimental data well.

The pseudo- second order kinetic model was proposed by Ho and McKay [34]. The rate-limiting phase, according to this hypothesis, is the sharing of electrons between the adsorbent and the adsorbate. The linearized form of this model is as follows:

$$\frac{t}{q_t} = \frac{1}{(k_2 . q_e^2)} + \frac{t}{(q_e)} \quad (2)$$

where k_2 represents the second order rate constant (g/(mg·min)) and t represents time (min). The experimental data follows the pseudo- first order reaction model if the chemical reaction is the rate-controlling step.

Table 1 Parameters of pseudo- first order and pseudo-second order reactions for adsorption MG on the AC1 and AC2

Parameter	Temperature (°C)					
	AC1			AC2		
	30	40	50	30	40	50
$q_{e,exp}$ ($mg.g^{-1}$)	75	75	75	30	40	50
Pseudo-first-order model						
k_1 (min^{-1})	0.444	0.891	0.447	0.024	0.048	0.043
$q_{e,cal}$ ($mg.g^{-1}$)	59.92	112.36	64.53	30.12	25.64	30.12
R^2	0.9958	0.9743	0.9957	0.7463	0.8899	0.7520
Pseudo-second-order model						
$k_2 x 10^3$ ($g.mg^{-1}.min^{-1}$)	0.126	0.221	0.104	0.02	0.004	1.125
$q_{e,cal}$ ($mg.g^{-1}$)	75.2	75.2	75.2	30.12	25.64	30.12
R^2	1	1	1	0.9999	0.9867	1

The MG adsorption characteristics on both AC1 and AC2 are presented in Table 1. Because R^2 was closer to 1.0, the experimental results suited the pseudo- second order kinetic model well. The development of interactions between MG and AC1, as well as one between MG and AC2, is the rate-limiting stage.

3.4 Adsorption isotherms

To better understand adsorption behaviour, two adsorption isotherm models (Langmuir and Freundlich isotherms) are employed to match the equilibrium data. The Langmuir isotherm [35] assumes of a homogeneous adsorbent surface with a finite number of identical sites. The linearized form of the Langmuir isotherm equation in found by:

$$\frac{C_e}{q_e} = \frac{C_e}{q_m} + \frac{1}{k_L q_m} \quad (3)$$

where q_m represents the maximal monolayer adsorption capacity (mg/ g) and k_L represents the Langmuir constant (L/g). The dimensionless constant "R_L" can be used to define the main features of the Langmuir isotherm. The RL is a separation factor or equilibrium parameter whose definition is as follows:

$$R_L = \frac{1}{1 + k_L . C_0} \quad (4)$$

The value of this parameter indicates whether the isotherm is irreversible (R_L = 0), favorable (0<R_L<1), linear (R_L = 1), or unfavorable (R_L>1).

The parameters derived from fitting equilibrium data to adsorption isotherm models are listed in Table 2. On both adsorbents, the MG adsorption closely followed the Langmuir isotherm model. This shows that the MG dyes create a monolayer on the AC1 and AC2 surfaces. Adsorption techniques such as physical and chemical adsorption result in monolayer coverage of dye molecules on the adsorbent. Monolayer physisorption occurred as a result of this experiment. The maximum monolayer adsorption capacities of the AC1 and AC2 were 136.99 and 68.97 mg/ g, respectively. The Freundlich isotherm produced n values ranging from 1 to 10, showing that adsorption is favorable. The maximum monolayer adsorption capacities of several adsorbents discovered in the related literature are summarized in Table 3. The maximum monolayer adsorption capacity found in this investigation appears to be comparable to that of other activated carbons.

Table 2 Isotherm constants and correlation coefficient for the adsorption of MG on the AC1 and AC2

Parameter	Temperature (°C)					
	AC1			AC2		
	30	40	50	30	40	50
Langmuir isotherm						
q_m (mg.g^{-1})	109.89	136.99	136.00	62.89	64.94	68.37
k_L (-)	1.32	0.90	1.40	0.6	0.6	0.6
R_L	0.06	0.02	0.01	0.03	0.03	0.03
R^2	0.9995	0.9960	0.9998	0.9634	0.9737	0.9612
Freundlich isotherm						
n (-)	4.70	2.71	2.96	2.33	1.97	1.89
k_f (mg.g^{-1})	54.47	57.13	65.76	23.14	22.73	22.69
R^2	0.9634	0.9737	0.9612	0.6595	0.7913	0.8077

Table 3 Maximum monolayer adsorption capacity of MG on various adsorbents

Adsorbent	q_m, mg/g	Reference
AC1	136.99	This study
AC2	68.97	This study
Potassium salts-activated carbon	167.0	[37]
Firminana simplex wood fiber	142.4	[38]
Activated carbon from rice husk	63.85	[39]
Chitosan ionic liquid beads	8.07	[40]
Activated carbon from *Borassus aethipum* flower	48.48	[41]
Activated carbon from groundnut shell waste	222.22	[42]
Banana peel	243.90	[32]

3.5 Adsorption mechanisms

The dye molecules' probable interactions with the adsorbent are depicted in Figure 9. Symbol 1 depicts the diffusion of MG dye molecules into the micropores of the AC1 and AC2. The AC1 and AC2 have the same average pore diameter of 1.80 nm, making them micropores (pore size less than 2 nm). This step is often delayed because it includes the influence of internal mass transfer resistance. Furthermore, a progressive increase in dye uptake with constant time can provide further support for pore diffusion in the second stage (see Figure 6).

The migration of MG dye molecules into the AC1 mesopores is seen in Symbol 2. The AC1's N_2 adsorption-desorption isotherm, which agreed with the N_2 isotherm of mesoporous materials [37], revealed the hysteresis loop. On the external surfaces, symbol 3 depicts the adhesions between hydrophobic regions of the MG dye molecules and the hydrophobic parts of the AC1 and AC2. It has been well documented that van der Waals forces are present in every molecule [43]. The electrostatic interactions between the MG molecules and carboxyl groups are represented by symbol 4. The hydrogen bonding between MG molecules and hydroxyl groups is seen in symbol 5. The rise in dye uptake with raising the initial pH of the solution suggests these interactions. Stronger electrostatic interactions are caused by a higher degree of dissociation of carboxyl and hydroxyl groups on the adsorbent's external surface [44].

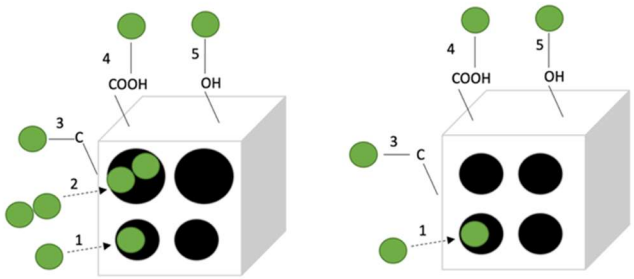

Figure 9 Adsorption Mechanisms of MG on AC1 (left) and AC2 (right)

4. Conclusions

The surface of bituminous coal activated carbon (AC1) has both mesopores and micropores, whereas the activated carbon from coconut shells (AC2) has mostly micropores. Both adsorbents have exterior surfaces with fixed negative charges that have a strong affinity for cationic compounds. The amount of MG dyes adsorbed rose as initial pH0 and contact duration increased but reduced when the initial dye concentration. The dye uptakes of both AC1 and AC2 are temperature independent. The maximum MG dye uptake was reported when the pH0 was 4.0-8.0, contact period of 30 minutes, C0 of 300 mg/L, and temperature of 30 - 50 °C. The Langmuir isotherm and pseudo-second order reaction models were used to predict the experimental results. In this investigation, monolayer physisorption happened. Because of the high adsorption capacity of MG dyes adsorbed on commercial AC1 and AC2, both are efficient adsorbents for removing cationic dyes liquid media.

Acknowledgements

The authors would like to express their gratitude to the Faculty of Engineering, Ubon Ratchathani University for the partial financial assistance, as well as the National Research Council of Thailand in 2011.

References

[1] Slama HB, Bouket AC, Pourhassan Z, Alenezi FN, Silini A, Cherif-Silini H. et al. Diversity of synthetic dyes from textile industries, discharge impacts and treatment methods. *Applied Sciences*. 2021;11(14): 6255.

[2] Khan S, Malik A. Toxicity evaluation of textile effluents and role of native soil bacterium in biodegradation of a textile dye. *Environmental science and pollution research international.* 2017; 25(5): 4446–4458.

[3] Sartape AS, Mandhare AM, Jadhav VV, Raut PD, Anuse MA, Kolekar SS. Removal of malachite green dye from aqueous solution with adsorption technique using *Limonia acidissima* (wood apple) shell as low cost adsorbent. *Arabian Journal of Chemistry*. 2019;10: S3229-S3238.

[4] Adeyi AA, Jamil SNAM, Abdullah LC, Choong TSY. Adsorption of malachite green dye from liquid phase using hydrophilic thiourea-modified poly (acrylonitrile-co-acrylic acid): kinetic and isotherm studies. *Journal of Chemistry.* 2019; Article ID 4321475.

[5] Ullah S, Rahman AU, Ullah F, Rashid A, Arshid A, Arshad T, et al. Adsorption of malachite green dye onto mesoporous natural inorganic clays: their equilibrium isotherm and kinetic studies. *Water*. 2021;13(7): 965.

[6] Piaskowski K, Swiderska-Dabrowska R, Zarzycki P K. Dye removal from water and wastewater using various physical, chemical, and biological processes. *Journal of AOAC International*. 2018; 101(5): 1371-1384.

[7] Katheresan V, Kansedo J, Lau SY. Efficiency of various recent wastewater dye removal methods: A review. *Journal of Environmental Chemical Engineering*. 2018. 6(4): 4676-4697.

[8] Ahmad A, Mohd-Setapar SH, Chuong CS, Khatoon A, Wani WA, Kumar R, et al. Recent advances in new generation dye removal technologies: novel search for approaches to reprocess wastewater. *RSC Advances*. 2015;5: 30801-30818.

[9] Cheng J, Zhan C, Wu J, Cui Z, Si J, Wang Q, et al. Highly efficient removal of methylene blue dye from an aqueous solution using cellulose acetate nanofibrous membranes modified by polydopamine. *ACS Omega*. 2020; 5(10): 5389-5400.

[10] Gan YX. Activated carbon from biomass sustainable sources. *C — Journal of Carbon Research.* 2021; 7(2): 39.

[11] Sajjadi B, Chen WY, Egiebor NO. A comprehensive review on physical activation of biochar for energy and environmental applications. *Reviews in Chemical Engineering.* 2019; 35(6): 735-776.

[12] Heidarinejad Z, Dehghani MH, Heidari M, Javedan G, Ali I, Sillanpaa M. Methods for preparation and activation of activated carbon: a review. *Environmental Chemistry Letters.* 2020; 18(2): 393–415

[13] Sun K, Leng CY, Jiang JC, Bu Q, Lin GF, Lu XC, et al. Microporous activated carbon from coconut shells produced by self-activation using the pyrolysis gases produced from them, that have an excellent electric double layer performance. *New Carbon Mater*. 2017; 32(5): 451-459.

[14] Umpuch C, Leesopha C, Nongsena P, Turongruang J, Puchongkawarin C. Adsorption of Rhodamine B dye onto activated carbon from coconut shell (in Thai). *Journal of Science and Science Education*. 2021; 4(1): 22-37.

[15] Hoang LP, Van HT, Nguyen TTH, Nguyen VQ, Thang PQ. Coconut shell activated carbon/$CoFe_2O_4$ composite for the removal of rhodamine B from aqueous solution. *Journal of Chemistry.* 2020; ID 9187960.

[16] Oribayo O, Olaleye OO, Akinyanju AS, Omoloja, KO, Williams SO. Coconut shell-based activated

carbon as adsorbent for the removal of dye from aqueous solution: equilibrium kinetics, and thermodynamic studies. *Nigerian Journal of Technology.* 2020; 39(4): 1076-1084.

[17] Lawtae P, Tangsathitkulchai C. A new approach for controlling mesoporosity in activated carbon by controlling mesoporosity in activated carbon by the consecutive process of air oxidation, thermal destruction of surface functional groups, and carbon activation (the OTA method). *Molecules*. 2021; 26(9): 2758.

[18] Kopac T, Sulu E, Toprak A. Effect of KOH treatment on bituminous coal for the effective removal of basic blue 41 dye from aqueous solutions. *Desalination and Water Treatment.* 2016; 57(59): 29007-29018.

[19] Qada ENE, Allen S, Walker GM. Adsorption of methylene blue onto activated carbon produced from steam activated bituminous coal: A study of equilibrium adsorption isotherm. *Chemical Engineering Journal.* 2006; 124(1): 103-110.

[20] Qu W, Yuan T, Yin G, Xu S, Zhang Q, Su H. Effect of properties of activated carbon on malachite green adsorption. *Fuel*. 2019;249: 45-53.

[21] Cychosz KA, Thommes M. Progress in the Physisorption characterization of nanoporous gas storage materials. *Engineering*. 2018; 4(4): 559-566.

[22] Serfin J, Narkiewicz U, Morawski AW, Wrobel RJ, Michalkiewicz B. Highly microporous activated carbons from biomass for CO_2 capture and effective micropores at different conditions. *Journal of CO_2 Utilization*. 2017; 18: 73-79.

[23] Sencan A, Kilic M. Investigation of the changes in surface area and FT-IR Spectra of activated carbons obtained from Hazelnut shells by physicochemical Treatment Methods. *Journal of Chemistry.* 2015; article ID 651651.

[24] Huang PH, Cheng HH, Lin SH. Adsorption of carbon dioxide onto activated carbon prepared from coconut shells. *Journal of Chemistry*. 2015; Article ID 106590.

[25] Mendez P, Nunez C, Cabrera-Pardo JR, Paz C, Barraza JM, Castillo R, et al. Adsorption ability of activated carbon obtained from sub-bituminous coal (LEBU CHILE) to capture trimethylamine. *Journal of the Chilean Chemical Society.* 2019; 64(3): 4582-4585.

[26] Song C, Wu S, Cheng M, Tao P, Shao M, Gao G. Adsorption studies of coconut shell carbons prepared by KOH activation for removal of Lead (II) from aqueous solutions. *Sustainability*. 2014; 6: 86-98.

[27] Tejada-Tovar C, Gonzalez-Delgado AD, Villabona-Ortiz A. Characterization of residual biomasses and its application for the removal of lead ions from aqueous solution. *Applied Sciences.* 2019; 9: 4486.

[28] Umpuch C. Removal of yellow20 dye from aqueous solution using organo-rice straw: characteristic, kinetic and equilibrium studies. *Engineering Journal.* 2015; 19(2): 59-69.

[29] Namdaung P, Umpuch C. Adsorption of reactive red 120 onto cationic surfactant intercalated montmorillonite clay. *Journal of Engineering and Innovation.* 2019; 12(2): 1-12.

[30] Elkady M, Shokry H, Hamad H. New activated carbon from mine coal for adsorption of dye in simulated water of multiple heavy metals in real wastewater. *Materials (Basel)*. 2020; 13(11): 2498.

[31] Kavci E. Malachite green adsorption onto modified pinecone: isotherm, kinetics and thermodynamics mechanism. *Chemical Engineering Communications.* 2021. 208(3); 318-327.

[32] Saechiam S. Sripongpun G. Adsorption of malachite green from synthetic wastewater using

banana peel adsorbents. *Songklanakarin Journal of Science and Technology*. 2019; 41(1): 21-29.

[33] Moussout H, Ahlafi H, Aazza M, Maghat H. Critical of linear and nonlinear equations of pseudo-first order and pseudo-second order kinetic models. *Karbala International Journal of Modern Science.* 2018; 4(2): 244-254.

[34] Azizian S. Kinetic models of sorption: a theoretical analysis. *Journal of Colloid and Interface Science*. 2004; 276(1): 47-52.

[35] Wang J, Guo X. Adsorption isotherm models: Classification, physical meaning, application and solving method. *Chemosphere*, 2019; 258: 127279.

[36] Firdaus PM, Wahyuningsih S, Nugrahaningtyas KD, Hidayat Y. Derivation and constants determination of the Freundlich and (fractal) Langmuir adsorption isotherms from kinetics. *IOP Conference Series: Materials Science and Engineering.* 333; 2018: 012010.

[37] Tang SH, Zaini MAA. Malachite green adsorption by potassium salts-activated carbons derived from textile sludge: Equilibrium, kinetics and thermodynamics studies. *Asia-Pacific Journal of Chemical Engineering*. 2016; 12(1), 159-172.

[38] Pan X, Zhang D. Removal of malachite green from water by Firmiana simplex wood fiber. *Electronic Journal of Biotechnology*. 2009; 12(4): 1-10.

[39] Sharman YC, Singh BU. Fast Removal of malachite green by adsorption on rice husk activated carbon. *The Open Environmental Pollution & Toxicology Journal.* 2019; 1: 74-78.

[40] Naseeruteen F, Hamid NSA, Suah FBM, Ngah WSW, Mohamod FS. Adsorption of malachite green from aqueous solution by using novel chitosan ionic liquid beads. *International journal of biological macromolecules*. 2018; 107(pt A): 1270-1277.

[41] Nethaji S, Sivasamy A, Thennarasu G, Saravanan S. Adsorption of malachite green dye onto activated carbon derived from *Borassus aethiopum* flower biomass. *Journal of Hazardous Materials.* 2010; 181(1-3): 271-280.

[42] Malik R, Ramteke DS, Wate SR. Adsorption of malachite green on groundnut shell waste based powdered activated carbon. *Waste Management*. 2007; 27: 1129-1138.

[43] Lee YC, Amini MHM. Sulaiman NS, Mazian M. Batch adsorption and isothermic studies of malachite green dye adsorption using *Leucaena leucocephala* biomass as potential adsorbent in water treatment. *Journal of Science and Technology.* 2018; 40(3): 563-569.

[44] Oyelude EO, Awadza JAM, Twumasi SK. Removal of malachite green from aqueous solution using pulverized teak leaf litter: equilibrium, kinetic and thermodynamic studies. *Chemistry Central Journal.* 2018;12: 81.